Science of the Total Environment 472 (2014) 681–694

Contents lists available at ScienceDirect

Science of the Total Environment

journal homepage: www.elsevier.com/locate/scitotenv

Corrosion and runoff rates of Cu and three Cu-alloys in marine environments with increasing chloride deposition rate

Inger Odnevall Wallinder [a,*], Xian Zhang [a], Sara Goidanich [b], Nathalie Le Bozec [c], Gunilla Herting [a], Christofer Leygraf [a]

[a] KTH Royal Institute of Technology, Div. Surface and Corrosion Science, Dr. Kristinas v. 51, SE-100 44 Stockholm, Sweden
[b] Department of Chemistry, Materials and Chemical Engineering "Giulio Natta", Politecnico di Milano, P.za Leonardo da Vinci 32, 20133 Milano, Italy
[c] French Corrosion Institute, 220 rue Pierre Rivoalon, 29200 Brest, France

HIGHLIGHTS

- Atmospheric corrosion of Cu, Cu15Zn, Cu4Sn and Cu5Al5Zn at decreasing coastal distance
- Decreasing corrosion rates with decreasing chloride load for all materials
- Flaking of outer patina constituents for Cu and Cu4Sn at sites of high chloride load
- Significantly lower release rates compared with corrosion rates
- Comparable long term release of Cu from the alloys due to similar outermost patina composition

ARTICLE INFO

Article history:
Received 21 July 2013
Received in revised form 11 November 2013
Accepted 16 November 2013
Available online 7 December 2013

Keywords:
Atmospheric corrosion
Chloride deposition
Corrosion rates
Patina evolution
Metal release
Copper alloys

ABSTRACT

Bare copper sheet and three commercial Cu-based alloys, Cu15Zn, Cu4Sn and Cu5Al5Zn, have been exposed to four test sites in Brest, France, with strongly varying chloride deposition rates. The corrosion rates of all four materials decrease continuously with distance from the coast, i.e. with decreasing chloride load, and in the following order: Cu4Sn > Cu sheet > Cu15Zn > Cu5Al5Zn. The patina on all materials was composed of two main layers, Cu_2O as the inner layer and $Cu_2(OH)_3Cl$ as the outer layer, and with a discontinuous presence of CuCl in between. Additional minor patina constituents are SnO_2 (Cu4Sn), $Zn_5(OH)_6(CO_3)_2$ (Cu15Zn and Cu5Al5Zn) and $Zn_6Al_2(OH)_{16}CO_3 \cdot 4H_2O/Zn_2Al(OH)_6Cl \cdot 2H_2O/Zn_5Cl_2(OH)_8 \cdot H_2O$ and Al_2O_3 (Cu5Al5Zn). The observed Zn- and Zn/Al-containing corrosion products might be important factors for the lower sensitivity of Cu15Zn and Cu5Al5Zn against chloride-induced atmospheric corrosion compared with Cu sheet and Cu4Sn.
Decreasing corrosion rates with exposure time were observed for all materials and chloride loads and attributed to an improved adherence with time of the outer patina to the underlying inner oxide. Flaking of the outer patina layer was mainly observed on Cu4Sn and Cu sheet and associated with the gradual transformation of CuCl to $Cu_2(OH)_3Cl$ of larger volume. After three years only Cu5Al5Zn remains lustrous because of a patina compared with the other materials that appeared brownish–reddish.
Significantly lower release rates of metals compared with corresponding corrosion rates were observed for all materials. Very similar release rates of copper from all four materials were observed during the fifth year of marine exposure due to an outer surface patina that with time revealed similar constituents and solubility properties.

1. Introduction

Copper in its pure or alloyed state forms a large group of industrially very important materials. Depending on alloying elements, the desirable properties range from high electrical conductivity, corrosion resistance, wear resistance, tensile strength, soldering and joining characteristics to appealing visual appearance. This study concerns the atmospheric corrosion of bare copper sheet and three commercial Cu-alloys exposed to four different levels of chloride deposition rates in a marine environment. As evidenced from a recent review (Sequeira,

* Corresponding author. Tel.: +46 8 7906621.
E-mail addresses: ingero@kth.se (I. Odnevall Wallinder), xianzh@kth.se (X. Zhang), sara.goidanich@polimi.it (S. Goidanich), nathalie.lebozec@institut-corrosion.fr (N. Le Bozec), herting@kth.se (G. Herting), chrisl@kth.se (C. Leygraf).

0048-9697
http://dx.doi.org/10.1016/j.scitotenv.2013.11.080

2011), the atmospheric corrosion of pure copper in chloride-dominating environments has been extensively studied whereas much less is known about Cu-alloys such as brass and bronze. Typical corrosion rates of bare copper sheet in marine environments have been reported around 1 μm y^{-1}, whereby the initial rate is higher and then declines with time due to the build-up of protective corrosion products (Leygraf and Graedel, 2000). In sheltered marine exposure conditions the evolution of corrosion products proceeds through the initial formation of cuprite (Cu_2O) which continues to grow during the entire exposure period. It continues with the formation of nantokite (CuCl) and commonly ends with atacamite or the isomorphous phase paratacamite ($Cu_2Cl(OH)_3$) as corrosion end products (Krätschmer et al., 2002). These corrosion products have all also been observed within the patina on bare copper at unsheltered marine exposure conditions, and formed in laboratory exposure conditions with humidified air and predeposited NaCl (Strandberg and Johansson, 1998). The same investigation showed the corrosion rate of copper to increase with the amount of deposited NaCl and with relative humidity (Strandberg and Johansson, 1998).

More detailed laboratory studies have considered the lateral variation in surface composition and in anodic and cathodic area distribution within and adjacent to individual NaCl-particles deposited on bare copper (Chen et al., 2005a,c) and zinc (Chen et al., 2008; Neufeld et al., 2002) surfaces, respectively. Spreading of the electrolyte turned out to create the formation of galvanic elements with a potential gradient between the central area of the droplet at the NaCl particle (the anodic area) and a so-called secondary spreading area at the periphery of the droplet (the cathodic area). The interplay between acidifying gases involved, SO_2 or CO_2, and the secondary spreading phenomenon turned out to be highly complex and dependent on the concentration of the gases involved. Corrosion products observed on copper at these conditions include Cu_2O, $Cu_2Cl(OH)_3$ and brochantite ($Cu_4SO_4(OH)_6$) and on zinc zincite (ZnO), hydrozincite ($Zn_5(CO_3)_2(OH)_6$) and simonkolleite ($Zn_5Cl_2(OH)_8 \cdot H_2O$). A limited number of more detailed studies on the influence of chlorides on Cu-alloys have been reported. By exposing a bronze (Cu20Sn5Pb) alloy to humidified air with both chlorides and NO_2 present it was found that NO_2 could act as a catalyst during the corrosion process resulting in a synergism between chlorides and NO_2 on the corrosion kinetics (Cao et al., 2009). CuCl, cassiterite (SnO_2) and lead oxide (PbO) were identified as the main constituents of the corrosion products. The same bronze alloy was also exposed to chlorides and bisulfite (HSO_3^-) ions, in which a synergistic effect between the ions was observed (Cao and Xu, 2006).

When exploring the fundamentals of chloride aerosols and their influence on the atmospheric corrosion of metals, the varying exposure conditions at marine sites add in complexity. In a series of papers, Cole et al. (2009, 2003, 2004) have developed a holistic model aiming at understanding the fundamentals of marine aerosols and their influence on corrosion of primarily zinc at different distances and conditions from the ocean coastal line. The important parameters that are considered are the production, transportation and deposition of aerosols, and factors that may influence the size and chemistry of aerosols. Morcillo and co-workers have reported another set of papers, (see e.g. Feliu et al., 1999; Morcillo et al., 2001), in which different parameters have been analyzed that may influence the deposition rate of chlorides on various metals. An interesting finding from both sets of papers is the conclusion of at least two decay functions of the chloride deposition rate versus distance from the coastal line, corresponding to two different sources for producing the aerosols, breaking surf and ocean whitecaps. Over the first 500 m from the coast the chloride deposition is initially very high but decays rapidly, whereas the decay from about 2 km and inward is lower closer to the coast and decreases less rapidly.

This study is part of a long-term project with an international industry consortium that aims at assessing and generating a comprehensive understanding of atmospheric corrosion and metal release processes of copper and copper-based alloys used in building applications. In this sub-project, bare Cu and three bare commercial Cu-based alloys (Cu15Zn, Cu4Sn and Cu5Al5Zn) have been exposed at unsheltered conditions for up to three years at four marine test sites in Brest, France, representing four distances from the coastal line with a large span in chloride deposition rates. The aim is to provide a unique understanding of the rate of patina formation and coloration of copper and copper-based alloys and how they are influenced by alloying elements and chloride deposition rates. The four test sites are characterized with respect to their predicted corrosivity following the ISO 9223 classification system (ISO, 2012a) and compared with measured rates at all sites. Changes in visual appearance and evolution of patina coloration are discussed in relation to patina constituents and characteristics. Differences in metal runoff are further discussed in relation to patina constituents at one of the sites with strong chloride influence.

The importance of exploring the influence of chlorides on atmospheric corrosion rates of metals is also justified by the prediction that future corrosion rates, at least in Europe, will be more dominated by chlorides in coastal or near-coastal areas than today because of the expected increase in relative importance of chlorides on corrosion effects with increasing temperature (Tidblad, 2012).

2. Experimental

2.1. Materials and exposure conditions

Copper sheet, Cu4Sn (96 wt.% Cu and 4 wt.% Sn), Cu15Zn (85 wt.% Cu and 15 wt.% Zn), and Cu5Al5Zn (89 wt.% Cu, 5 wt.% Al, 5 wt.% Zn, 1 wt.% others) were exposed at outdoor unsheltered conditions (45° and 90° from the horizontal, facing south) at the marine site of Brest, France, for 3 and 6 months, and 1, 2 and 3 years (starting from Nov 2009). Information on bulk alloy composition of the exposed materials is given in Table 1. Four different sites of increasing distance from the coastal line in the Brest region, France were selected (site 1 — Military harbor: <5 m; site 2 — St. Anne: 20–30 m; site 3 — St Pierre: 1.5 km; site 4 — Langonnet: 40 km). The location of the sites is shown in Fig. 1. Daily deposition rates of chlorides were measured with the wet candle technique on site following the ISO 9225 standard (ISO, 2012a). Measurements of temperature and relative humidity were also performed.

Samples were exposed at each site at different periods for ex situ surface analysis and corrosion rate measurements. Metal runoff measurements were performed on single sided samples sized 300 cm^2 at site 2, an exposure initiated prior to the corrosion rate and patina formation study (Cu sheet: June 2004; the alloys: Nov 2007). All samples were exposed as-received (to mimic commercial surfaces) after surface degreasing with acetone/isopropyl alcohol and drying with cold nitrogen gas. More detailed information is given elsewhere (Goidanich et al., 2011).

Cross-sections of the exposed samples were prepared by embedding the samples into a conductive polymer followed by polishing with 0.25 μm diamond paste and subsequent polishing using OP-S suspension (Struers A/S, Denmark) and water for 15 min to obtain a near mirror like cross-sectional surface.

2.2. Corrosion rate and metal runoff measurements

Continuous sampling of metal-containing runoff water was conducted on single sided surfaces, inclined 45° from the horizontal facing south, following the guidelines of the ISO 17752 standard (ISO, 2012b)

Table 1
Bulk alloy composition (wt.%).

Material	Cu	Sn	Zn	Al	Fe	S	Ni	P	Others
Cu	99.98	–	–	–	–	–	–	0.02	–
Cu4Sn	96.19	3.66	0.03	–	0.004	0.004	0.02	0.07	0.023
Cu15Zn	85.36	0.006	14.58	–	0.02	–	0.02	–	0.014
Cu5Al5Zn	88.82	0.93	4.88	4.84	0.46	0.001	0.01	0.005	0.054

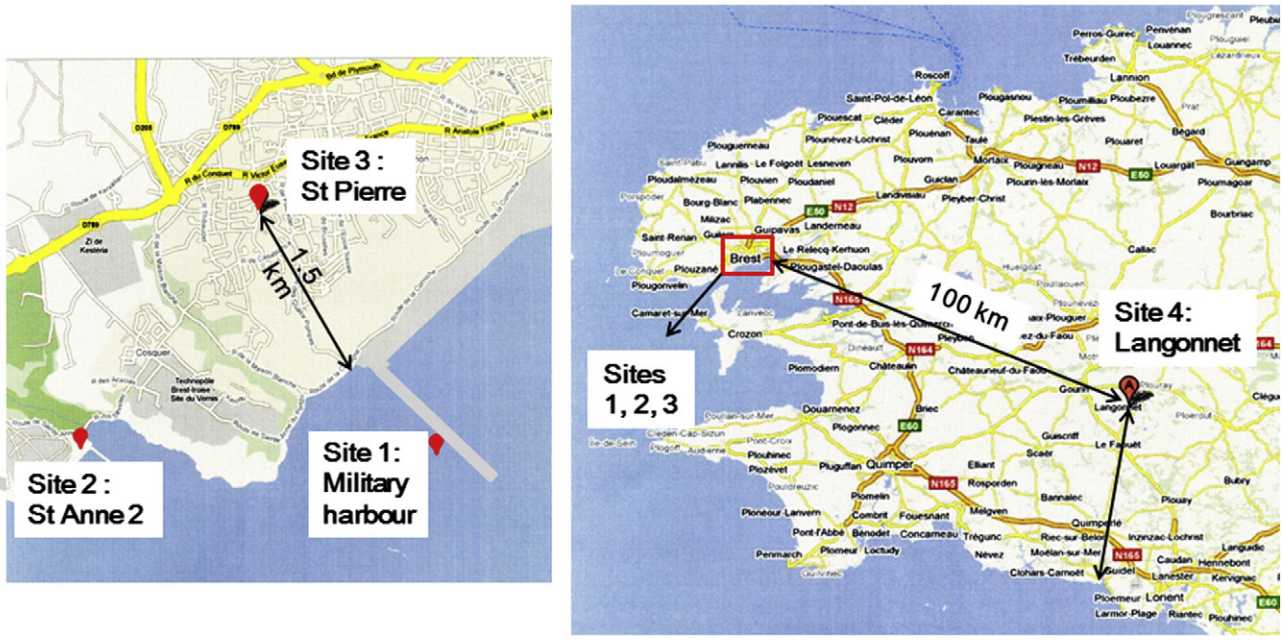

Fig. 1. Maps showing the four different exposure sites in the Brest region, France.

for metal runoff measurements. Samples for corrosion rate measurements were exposed according to ISO 9226 standard (ISO, 2012c). Corrosion rate measurements were conducted by stripping corrosion products from the surfaces by using amidosulfonic acid. The experimental procedure is given elsewhere (He et al., 2001). All metal runoff measurements were conducted by means of AAS (atomic absorption spectroscopy) with Perkin Elmer AAnalyst 800 at standard operational conditions. The parallel background concentration (blank) of metals was determined for runoff water collected from a bare Plexiglas fixture. Analyses of released copper and zinc were performed using the flame mode AAS, whereas released concentrations of tin, aluminum and iron were determined with graphite furnace AAS (GF-AAS) due to their low concentrations. Prior to analysis, the runoff water was acidified to a pH less than 2 to ensure complete dissolution of potentially formed complexes. Three replicate readings were made for each sample and control samples were run consecutively during the analysis (every 10^{th} sample). Detailed information is given elsewhere (Goidanich et al., 2011). Limits of detection for analysis of copper, zinc, tin, aluminum and iron in solution were 0.006, 0.003, 0.002, 0.003, 0.002 mg L^{-1}, respectively.

2.3. Surface and patina analysis

2.3.1. Stereomicroscopy

Stereomicroscopy imaging was employed to document surface appearance by using a M205C Stereo Microscope with a Leica DFC 290 video camera, using a D65 reference light source applied at 10° at a magnification of 40×.

2.3.2. SEM/EDS (scanning electron microscopy and energy dispersive spectroscopy)

SEM/EDS (*Scanning electron microscopy and energy dispersive spectroscopy*) analysis was conducted to document the morphology of corrosion products within the patina and to obtain elemental information. Cross-sections were analyzed using a LEO 1530 instrument with a Gemini column, upgraded to a Zeiss Supra 55 (equivalent) and an EDS X-Max SDD (Silicon Drift Detector) 50 mm^2 detector from Oxford Instruments. Surface analysis was performed using a FEI-XL 30 Series instrument, equipped with an EDAX Phoenix EDS system with an ultra-thin windows Si–Li detector.

2.3.3. FTIR (Fourier transform infrared reflection spectroscopy)

FTIR (*Fourier transform infrared reflection spectroscopy*) measurements were employed to identify functional groups within the patina using a Thermo Nicolet 6700 with DTGS detector (4000–400 cm^{-1}), coupled with a Thermo Nicolet Continuum FTIR microscope with MCT detector (4000–600 cm^{-1}). The spectra were collected from powder scraped from the surface.

2.3.4. CRM (confocal Raman microspectroscopy)

CRM (*confocal Raman microspectroscopy*) measurements were carried out to display the lateral distribution of functional groups representative for different corrosion products within the patina by using a WITec alpha300 system equipped with a laser source of wavelength 532 nm. A Nikon NA0.9 NGC objective was used for the measurements with a lateral resolution of approximately 300–400 nm.

2.3.5. GDOES (glow discharge optical emission)

GDOES (*glow discharge optical emission*) measurements were used to provide elemental depth information by using a Leco GDS 850 instrument. A circular area with a diameter of 4 mm was continuously

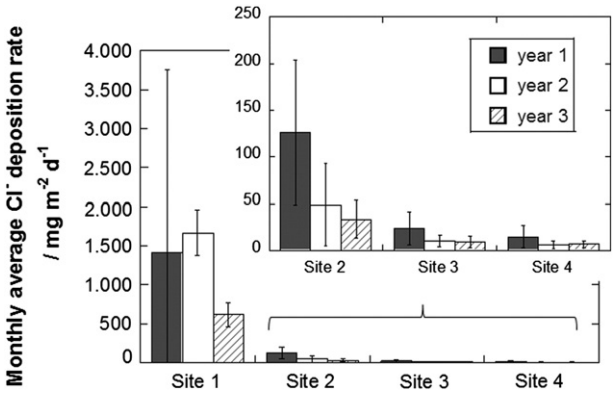

Fig. 2. Monthly average rates based on daily deposition rates of chlorides (mg m^{-2} d^{-1}) measured with the wet candle technique at the four test sites of increasing distance from the coastal line in the Brest region, France, during three years of exposure (Nov. 2009–Nov. 2012).

sputtered using Ar plasma at a potential of 700 V and a current of 20 mA. The Ar pressure varied between 6 and 7.5 Torr.

2.3.6. XPS (X-ray photoelectron spectroscopy) compositional

XPS (*X-ray photoelectron spectroscopy*) *compositional* measurements of the outermost patina were performed after 1, 2, and 3 years of exposure for all samples at site 1. XPS spectra were recorded at different positions using a Kratos AXIS UltraDLD X-ray photoelectron spectrometer (Kratos Analytical, Manchester, UK) using a monochromatic Al x-ray source. The analysis area was below about 1 mm^2 (most of the signal is from an area of 700 × 300 μm) collecting wide spectra and detailed high resolution spectra of C1s, O1s, Cu2p, Zn2p, Sn 3d, Fe2p, and Al2p.

2.3.7. GIXRD (grazing incidence X-ray diffraction)

GIXRD (*Grazing Incidence X-ray diffraction*) analysis was performed to identify crystalline corrosion products within the patina by using an X'pert PRO PANalytical system, equipped with an x-ray mirror (CuKα radiation) and a 0.27° parallel plate collimator on the diffracted side. Analysis was made on a 1 × 1 cm large surface area at a grazing angle of 88° versus the surface.

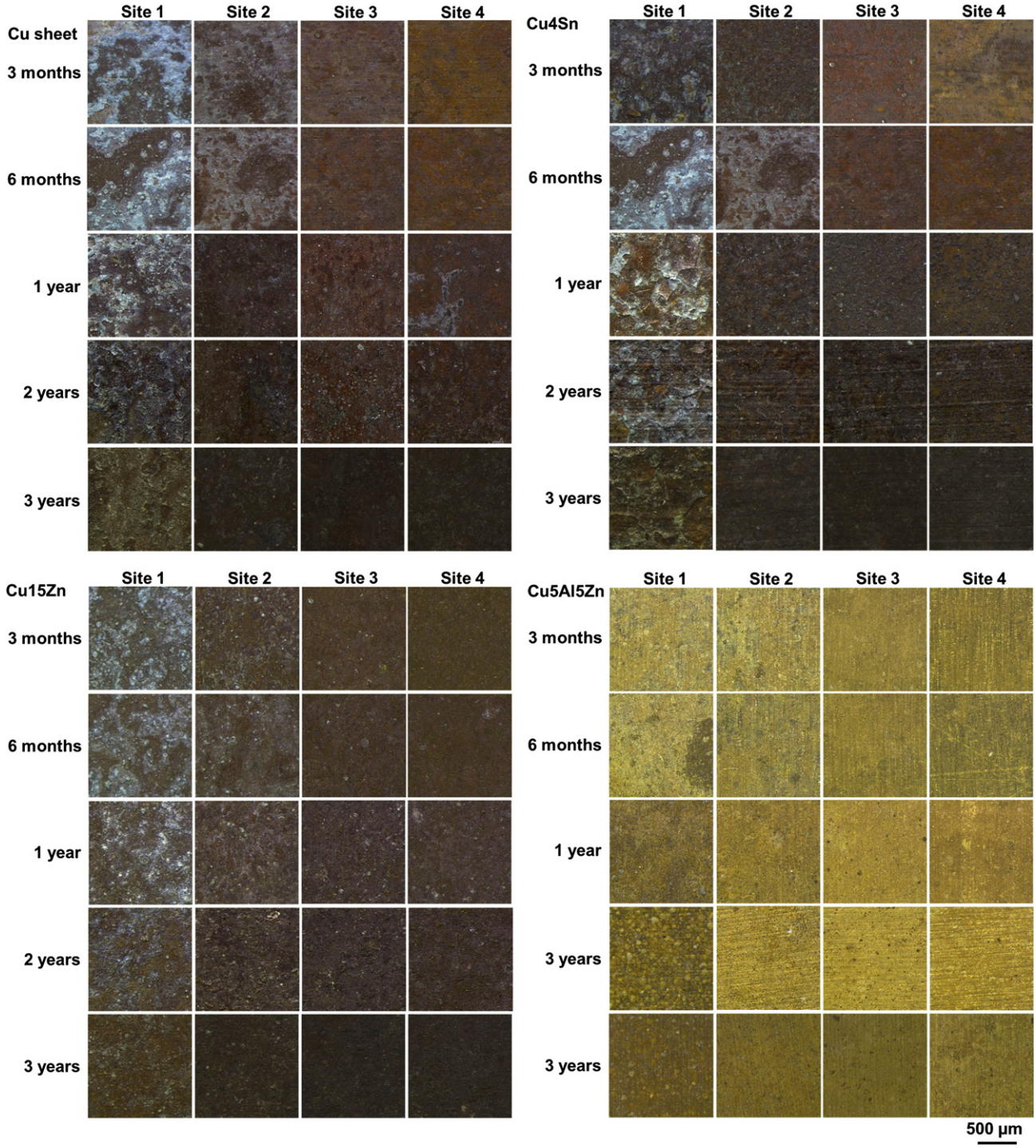

Fig. 3. Changes in visual appearance of copper sheet (Cu sheet), and the copper-based alloys (Cu4Sn, Cu15Zn, Cu5Al5Zn) upon unsheltered exposure for 3, 6 months, 1, 2 and 3 years at the four outdoor sites of increasing distance from the coastal line in the Brest region, France.

3. Results and discussion

3.1. Visual appearance of Cu and Cu-based alloys at marine exposure sites of varying deposition rates of chlorides

Copper sheet (Cu sheet) and three copper-based alloys (Cu4Sn, Cu15Zn, Cu5Al5Zn) were exposed for 3 months, 6 months, 1, 2 and 3 years at unsheltered marine conditions (45°and 90° from the horizontal, facing south) at four different sites of increasing distance from the coastal line (site 1: <5 m; site 2: 20–30 m; site 3: 1.5 km; site 4: 40 km). Measured deposition rates of chlorides substantially decreased with increased distance from the sea shore: site 1 ≫ site 2 ≫ site 3 > site 4, Fig. 2, a trend prevailing throughout the entire three-year exposure period. The first year of exposure was characterized by several autumn storms with significantly higher deposition rates of chlorides (large spread in results) compared with the other years, which explains the deviation in results on the monthly mean values. Median deposition rates of chlorides were approximately 6 to 7 times lower at site 2 compared with site 1 for all three years of exposure. Even lower median deposition rates of chlorides were observed for the other sites compared with site 1, 30–45 times lower at site 3, and 40–70 times lower at site 4.

Differences in chloride deposition rates were reflected in the surface appearance of the exposed materials, as illustrated in Fig. 3 after 3 - months, 6 months, 1, 2 and 3 years for each material. Initially, spatially heterogeneous surface appearances were evident for all materials. Greenish–bluish corrosion products were non-homogeneously distributed along the surfaces of Cu sheet, Cu4Sn and Cu15Zn at sites 1 and 2. After 3 years, the color of Cu, Cu4Sn and Cu15Zn reached a more brown-greenish appearance. The visual blue-greenish appearance was furthermore reduced with increasing distance from the coastal line. No blue-greenish corrosion products were visually observed on the Cu5Al5Zn-alloy at any sites. However, a pronounced formation of corrosion products influencing the surface appearance was evident, in particular at sites 1 and 2, which gradually reduced its lustrous appearance.

In the following, emphasis will be placed on the influence of chloride deposition rates on corrosion rates (metal loss), patina characteristics and metal release rates, starting with a corrosivity classification of the test sites.

3.2. Corrosivity classification of the test sites according to ISO 9223

The ISO standard 9223 (ISO, 2012d) is a classification system in which a given exposure site can be categorized with respect to corrosivity of carbon steel, zinc, copper and aluminum in two principally different ways. The first way is by directly measuring the corrosion effects during one year of exposure whereby the corrosion effects fall into one of five categories from C_1 (lowest) to C_x (highest). The second is by predicting the corrosivity through three environmental parameters: time of wetness (TOW) with five categories (τ_1 to τ_5), SO_2 concentration with four categories (P_0 to P_3) and air salinity in terms of the chloride deposition rate with four categories (S_0 to S_3). Further details are given in the standard (ISO, 2012d).

With similar time of wetness values (4800–5100 h/year), all sites (1–4) are categorized as τ_4. In reality, due to further chemical condensation by e.g. deposited chlorides and sulfates from sea-water aerosols, adsorbed molecular water layers, corrosion product formation and direct moisture precipitation of ocean spray, dew and rain, surface wetness will be even higher and all sites categorized as τ_5. The SO_2-concentration is at all four sites low, less than 2 μg/m^3, far below the upper limit of 12 μg m^{-3} for the P_0 category, and therefore all four sites have been categorized as P_0.

Fig. 4 displays monthly mean variations in chloride deposition rates, based on daily measurements using the wet candle method, for each site (1–4) during the first year of exposure. Strong monthly variations were observed between the sites and reflect the distance from the coast. Given the intervals of chloride deposition rates, site 1 may be categorized as S_3 (300–1500 mg m^{-2} d^{-1}), site 2 as S_2 (60–300 mg m^{-2} d^{-1}), and sites 3 and 4 as S_1 (30–60 mg m^{-2} d^{-1}).

The resulting estimated corrosivity based on data for the first year of exposure for site 1 was C_5, corresponding to a predicted copper corrosion rate of more than 25 g m^{-2} y^{-1}, in good agreement with a measured corrosion rate of 24.4 g m^{-2} y^{-1}. The corrosivity of site 2 was categorized as either C_3 or C_4, whereas sites 3 and 4 were classified as C_3. Table 2 displays that these estimated values corresponded very well with measured corrosion rates.

Test sites 1 to 4 exhibited similar time of wetness and SO_2 concentration but strong variations in chloride deposition rates that reflect the distance from the coastal line. Estimated corrosion rates according to ISO 9223 standard were in reasonable agreement with measured corrosion rates (varying by almost a factor of 3 between test sites 1 and 4) during the first year of exposure.

3.3. Observed corrosion rates of Cu and Cu-based alloys at all test sites

Measured average annual corrosion rates for Cu sheet and the three copper-based alloys (Cu4Sn, Cu15Zn and Cu5Al5Zn) exposed at 45° from the horizontal, facing south, are presented in Fig. 5 after the first, second and third years of exposure.

From the figures it is evident that the corrosion rates of all three Cu-based alloys follow the same trend as for bare Cu sheet with decreasing corrosion rates with increasing distance from the coastal line, i.e. with lower chloride deposition rate. Observed corrosion rates at test site 1 span from 38.3 g m^{-2} y^{-1} for Cu4Sn, over 24.4 g m^{-2} y^{-1} for Cu sheet, 19.4 g m^{-2} y^{-1} for Cu15Zn to 4.1 g m^{-2} y^{-1} for Cu5Al5Zn, i.e. a factor of almost ten from the lowest to the highest rates during the first year. This factor remained almost the same (Cu4Sn — the highest, Cu5Al5Zn — the lowest) when considering average corrosion rates after the second and the third years of exposure at test site 1. Literature findings have previously classified the corrosion rates of copper-based alloys into two general categories: alloys that corrode with a moderate rate such as tin bronzes, and alloys corroding with a slower rate including brass (Davis, 2001). Higher corrosion rates for Cu4Sn compared with those of Cu sheet and Cu15Zn are consistent with previous long-term exposure findings (up to 20 years) at marine sites (e.g. Costas, 1982; Holm and Mattson, 1982). The order in corrosion rates between the materials was not always the same at the other test sites and suggests that the protective ability of the patina formed differs not only between the materials, but also with the actual chloride deposition rate. Reduced average corrosion rates with time persisted during the whole three-year exposure period for all materials and test sites.

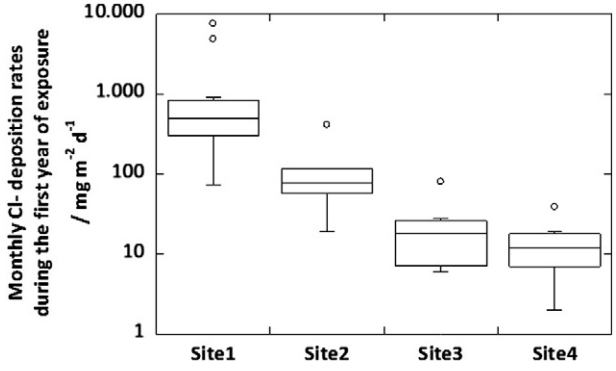

Fig. 4. Monthly mean daily deposition rates of chlorides measured with the wet candle technique at the four test sites, located at increasing distance from the coastal line in Brest, France, during the first year of exposure (Nov 2009–Nov 2010). 50% of all data is comprised within the box with the median value presented as a line. Sampling periods with deposition rates higher than 1.5 times the range of the box are presented as individual points.

Table 2
From left to right: site number, environmental parameters τ_n, P_n and S_n, estimated corrosivity C_n with corresponding corrosion rate (C_R) interval, and measured corrosion rate of copper sheet (inclined 45° from the horizontal, facing south) during the first year of unsheltered exposure at sites 1–4.

Site	Time of wetness TOW (τ_n)	SO_2 concentration (P_n)	Chloride deposition rate (S_n)	Estimated corrosivity category and corrosion rate (C_n; C_R g/m^2/y)	Corrosivity category and measured first year corrosion rate (C_n; g/m^2/y)
1	$\tau_4\tau_5$	P_1	S_3	$C_{5\ (very\ high)}$; $C_R > 25$	C_4–C_5; 24.4
2	$\tau_4\tau_5$	P_1	S_2	$C_{3\ (medium)}$; $5 < C_R \leq 12$ or $C_{4\ (high)}$; $12 < C_R \leq 25$	C_4; 16.3
3	$\tau_4\tau_5$	P_1	S_1	$C_{3\ (medium)}$; $5 < C_R \leq 12$	C_3–C_4; 12.2
4	$\tau_4\tau_5$	P_1	S_1	$C_{3\ (medium)}$; $5 < C_R \leq 12$	C_3; 8.9

In agreement with literature findings that report more rapid corrosion of horizontal and inclined surfaces compared with vertical surfaces (Cramer et al., 2002; Mattsson, 1980), observed corrosion rates for all materials were generally lower when exposed at 90° from the horizontal as compared with 45° (data not shown). The only exception was the Cu5Al5Zn alloy that only showed small differences in observed corrosion rates between the two inclination angles.

3.4. Patina formation and characteristics on Cu and Cu-based alloys at site 1 with high deposition rates of chlorides

In-depth corrosion product analyses were conducted at site 1 after 3 months, 6 months, 1, 2 and 3 years to assess the evolution of patina constituents. As expected from literature findings (e.g. De la Fuente et al., 2008; Ghoniem, 2011), copper revealed a porous inner (brownish) non-even layer (2–6 μm in thickness after 1 and 3 years) predominantly composed of copper-rich oxides and an outer (blue-greenish) layered and poorly adherent patina with chlorine-rich corrosion products. The outer layer became more compact and adhering to the underlying oxide with time, as displayed in Fig. 6 after 1 and 3 years. Despite a poorly adherent heterogeneous outer layer, the barrier properties of the corrosion patina improved after 3 years of exposure, as evidenced from corrosion rate findings, see Fig. 5.

Confocal Raman measurements performed on the cross-section of copper after 3 years clearly distinguished the two-layer structure with cuprite, Cu_2O (main bands at 225, 425, 645 cm^{-1}) (Kosec et al., 2012) in the inner layer and paratacamite, $Cu_2(OH)_3Cl$ (main bands at 520, 960, 3360, 3450 cm^{-1}) (Frost, 2003), the predominating constituent of the outer layer, Fig. 7.

Crystalline cuprite and paratacamite, $Cu_2(OH)_3Cl$, were also confirmed by means of GIXRD and FTIR measurements. The additional presence of atacamite cannot be excluded. Cross sectional elemental studies by means of EDS revealed chlorine both within the cuprite layer and at the cuprite/paratacamite interface. Similar observations were evident after 2 and 3 years of exposure. XRD measurements performed immediately after 3 months of exposure indicated the strongest diffraction peak of nantokite, CuCl. Due to the lack of additional peaks, its presence could not be unambiguously confirmed. The presence of nantokite within the patina was indicated by FTIR and Raman findings when comparing peak positions with spectra generated for artificial nantokite. However, due to the documented lack of stability of nantokite in humid environments (Chen et al., 2005b; Hayez et al., 2005), and its rapid transformation into paratacamite or its other isomorphous phases

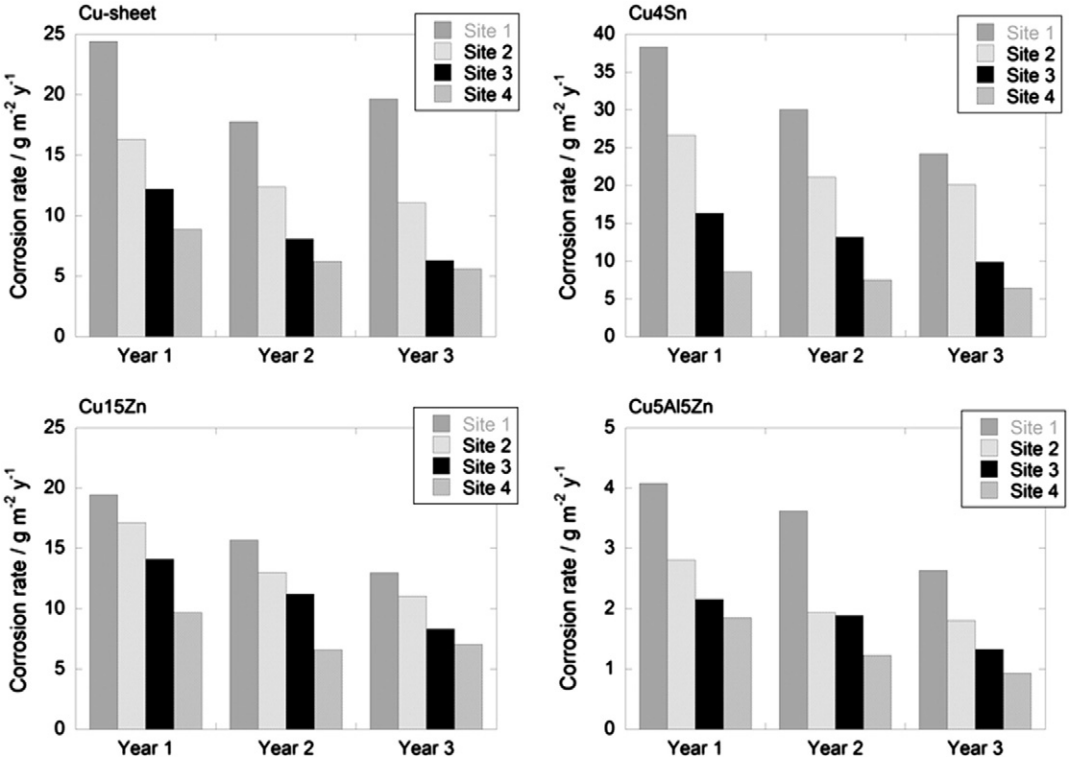

Fig. 5. Average annual corrosion rates determined for copper sheet and the three copper-based alloys (Cu4Sn, Cu15Zn and Cu5Al5Zn) after 1, 2 and 3 years of unsheltered exposure (45° from the horizontal, facing south) at the four test sites of decreasing chloride deposition rates with increasing coastal distance.

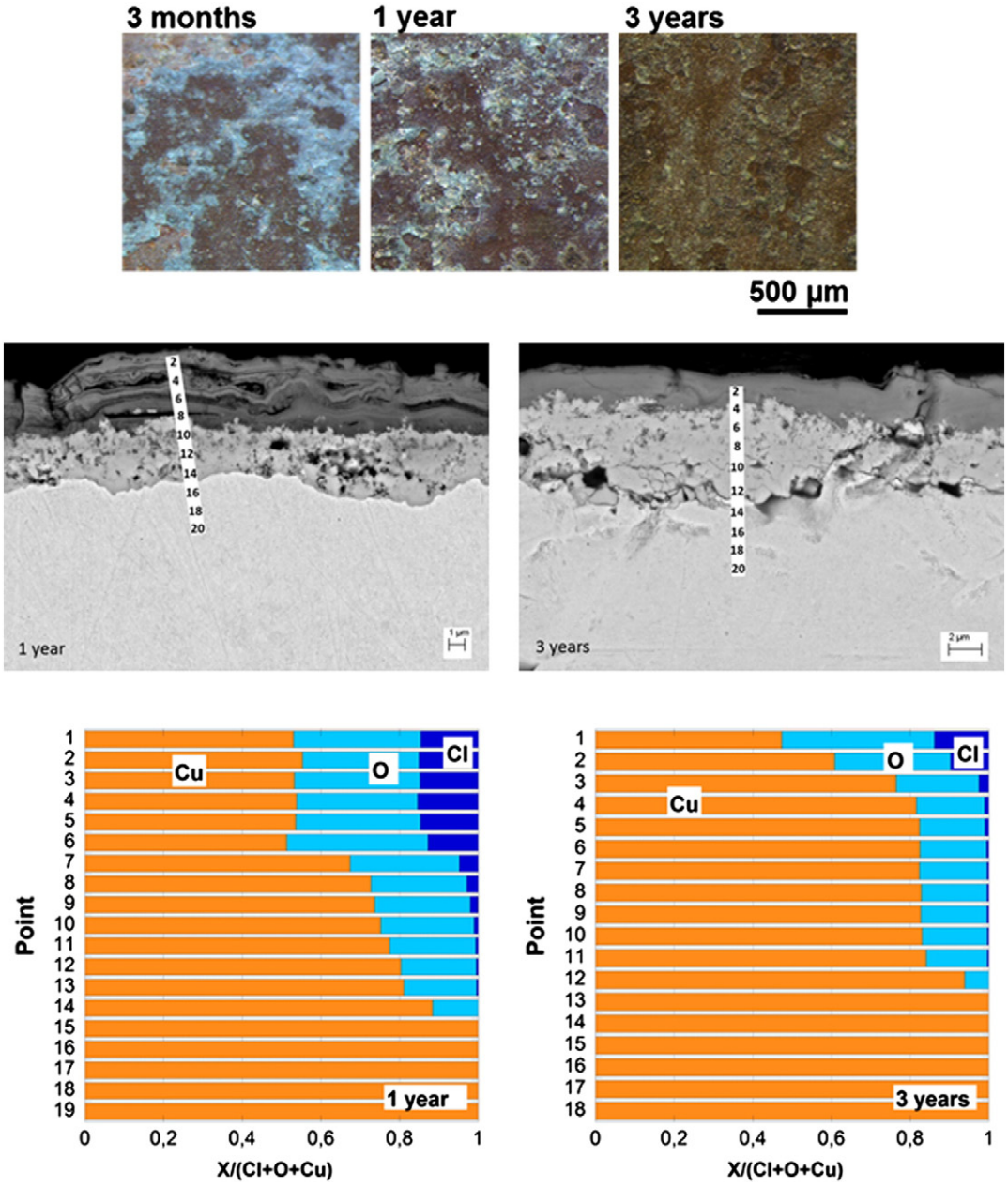

Fig. 6. Changes in visual appearance of copper sheet illustrated after 3 months, 1 and 3 years of exposure at site 1 (high deposition rates of chlorides) (top) and cross-sections of the corrosion patina after 1 and 3 years (middle) and corresponding relative elemental mass distribution based on EDS analysis (bottom).

(Krätschmer et al., 2002; Scott, 2002), its presence could not be confirmed. A more detailed investigation on nantokite formation and transformation in chloride rich environments will follow in a next-coming paper by the authors.

Similar measurements on Cu4Sn revealed a patina with a significantly thicker inner layer (10–20 µm after 1 year) compared with Cu sheet that contained streaks of oxidized copper and tin-rich corrosion products. Similar to findings for Cu sheet, chlorine was integrated within this inner layer and in a poorly adherent outer blue-greenish patina layer. The same observations were made after 2 and 3 years, Fig. 8. Cuprite and paratacamite (and possibly atacamite) were confirmed by means of GIXRD and FTIR and the presence of nantokite indicated (cf. copper sheet). The presence of tin within the inner layer (not specifically at the bulk/patina interface) suggests the additional presence of tin oxides, most probably SnO_2, an oxide previously identified in the patina of bronze in chloride rich environments (e.g. Constantinides et al., 2002; Ospitali et al., 2012). However, its presence did not reduce the corrosion rate of Cu4Sn, cf. Fig. 5 opposite to findings for environments of low chloride contents (Scholes and Jacob, 1970; Holm and Mattsson, 1982; Goidanich et al., 2008).

The occurrence of streaks of tin oxides within the relatively thick inner layer of cuprite was also confirmed by GDOES measurements showing an enrichment of tin compared to the bulk alloy content (4 wt. %) in certain streaks within the patina (data not shown).

Both Cu sheet and Cu4Sn revealed poorly adherent corrosion products that easily detached (spalled) in flakes from the surface. Flaking of corrosion products formed on copper-based alloys exposed in marine environments has been reported elsewhere (Scholes and Jacob, 1970). The high extent of spalling was attributed to the porous structure of the patina and the presence of nantokite within the patina.

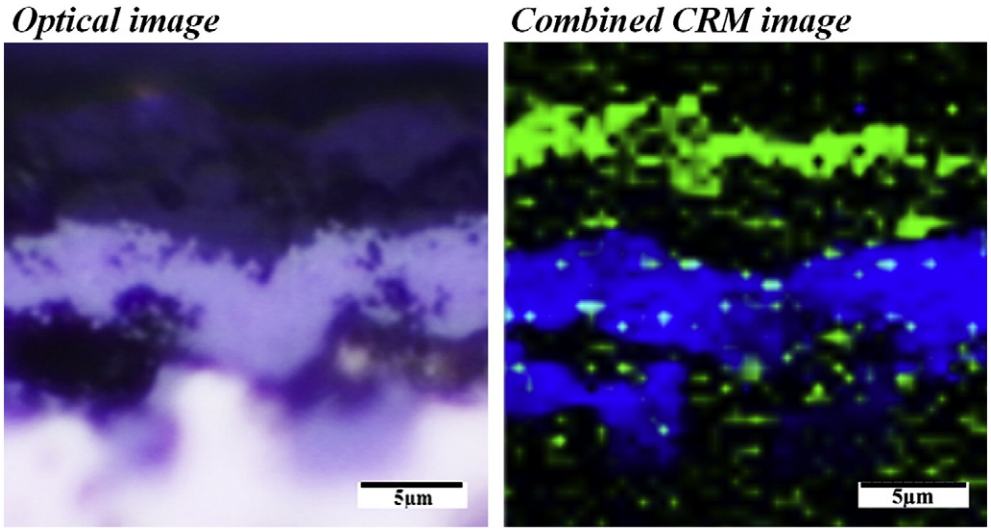

Fig. 7. Optical image and combined Raman mapping image obtained with CRM of Cu_2O band (blue inner layer, integrated between 175 and 275 cm^{-1}), and the OH band in $Cu_2(OH)_3Cl$ (green outer layer, integrated between 3300 and 3500 cm^{-1}), of cross-section of corrosion patina formed on Cu sheet after 3 years exposure at site 1.

Nantokite has been reported as an important phase for accumulating chloride ions at the patina/copper interface that react with cuprous ions from dissolved cuprite (Krätschmer et al., 2002; Watanabe et al., 2007). Initially formed nantokite easily transforms to paratacamite by reaction with moisture and oxygen, resulting in an expanded volume within the patina. This created physical stress within the porous patina, leading to severe flaking of corrosion products for Cu sheet and Cu4Sn.

No significant degree of spalling of loosely adherent corrosion products was evident for the Cu15Zn alloy. Cross-sectional studies revealed a non-uniform, relatively thin (1–5 μm), inner layer covered by a relatively dense, partly cracked, blue-greenish chlorine-rich patina.

Elemental analysis of cross-sections by means of EDS revealed the presence of zinc-rich corrosion products within the patina, both close to the bulk alloy/patina interface and within streaks, predominantly beneath the outer layer of paratacamite, Fig. 9. These findings were supported by GDOES observations, and Fig. 11 (left) GIXRD confirmed the presence of hydrozincite, $Zn_5(CO_3)_2(OH)_6$, zincite, ZnO and paratacamite in the outer layer. Surface sensitive measurements with XPS revealed a gradually reduced surface coverage of zinc-rich corrosion products with time showing a predominant copper-rich surface after three years (a Cu/Cu + Zn mass ratio increasing from 0.85 ± 0.05 to 1.0 after 1 and 3 years of exposure, respectively). However, literature findings have shown that zinc can stabilize paratacamite as zincian paratacamite ($(Cu, Zn)_2(OH)_3Cl$), a mixed copper–zinc chloride-rich corrosion product (Bertolotti et al., 2012; Scott, 2000). Its presence could however not be confirmed. The presence of zinc within the blue-greenish outer layer on Cu15Zn may indicate the formation of more stable zinc-rich corrosion products within the patina compared with copper-rich corrosion products. Such a stabilization may form a more compact patina layer on Cu15Zn compared with Cu sheet and Cu4Sn and reduce the extent and ability of dissolved cuprous ions and chloride ions to form CuCl, and thereby the extent of flaking.

The formation rate of corrosion products on the Cu5Al5Zn alloy was, in agreement with measured corrosion rates, significantly slower compared with Cu sheet and the other alloys, as evidenced by the relatively thin (1–2 μm) patina layer. Similar to Cu sheet, Cu4Sn and Cu15Zn, chlorine was predominantly present in the outermost patina layer, however without showing any blue-greenish appearance. Tin-, zinc-, aluminum-, and copper-rich phases were observed within the patina and at the bulk/patina interface, Fig. 10. According to GDOES findings tin was predominantly enriched within the patina and at the bulk/patina interface. Aluminum, zinc and iron were enriched compared to the bulk content to different extent at the bulk/patina interface. The depth profile is illustrated for zinc and tin in Fig. 11. Cuprite was identified by means of GIXRD in the inner layer and paratacamite in the outer layer. Simonkolleite ($Zn_5Cl_2(OH)_8 \cdot H_2O$) and/or $Zn_2Al(OH)_6Cl \cdot 2H_2O$/$Zn_6Al_2(OH)_{16}CO_3 \cdot 4H_2O$ may be possible additional patina constituents as their main diffraction peak was observed. However, due to the lack of additional peaks, their presence could not be confirmed.

A compilation of corrosion products identified within the patina of copper sheet and the copper-based alloys is given below based on the different analytical techniques employed. Corrosion products given in italic are not unambiguously identified. They could be possible phases, however, mainly with reference to earlier published studies mentioned in the Introduction section.

Cu sheet Cu_2O, CuCl, $Cu_2(OH)_3Cl$
Cu4Sn Cu_2O, *CuCl*, $Cu_2(OH)_3Cl$, *SnO_2*
Cu15Zn Cu_2O, *CuCl*, $Cu_2(OH)_3Cl$, ZnO, $Zn_5(OH)_6(CO_3)_2$
Cu5Al5Zn Cu_2O, *CuCl*, $Cu_2(OH)_3Cl$, *$Zn_5(OH)_6(CO_3)_2$*, $Zn_5(OH)_8Cl_2 \cdot H_2O$ and/or $Zn_6Al_2(OH)_{16}CO_3 \cdot 4H_2O$/$Zn_2Al(OH)_6Cl \cdot 2H_2O$, *$Al_2O_3$*

This study suggests that the zinc-rich phases within the patina of Cu15Zn ($Zn_5(OH)_6(CO_3)_2$), and Cu5Al5Zn ($Zn_5(OH)_8Cl_2 \cdot H_2O$ and/or $Zn_6Al_2(OH)_{16}CO_3 \cdot 4H_2O$/$Zn_2Al(OH)_6Cl \cdot 2H_2O$) alone or in combination may act as a protective barrier against chloride-induced corrosion. The importance of $Zn_5(OH)_6(CO_3)_2$ on galvanized steel and zinc sheet in chloride-rich environments has previously been suggested by Cole et al. (2009). Similar observations have been identified for $Zn_6Al_2(OH)_{16}CO_3 \cdot 4H_2O$ on zinc–aluminum based alloys (Volovitch et al., 2011; Zhang et al., 2013). However, the same compound has proven poor barrier properties and important metal loss for zinc–magnesium–aluminum coatings in low CO_2 atmospheres (LeBozec et al., 2013). Hydrozincite has been proposed to be stabilized in the secondary spreading region of deposited chlorides, and will protect the zinc surface from further corrosion due to its relatively high stability under given exposure conditions (Cole et al., 2009). The suggestion that hydrozincite and/or $Zn_6Al_2(OH)_{16}CO_3 \cdot 4H_2O$/$Zn_2Al(OH)_6Cl \cdot 2H_2O$ have a positive effect to reduce the influence of chlorides does not rule out the possible positive influence of also other corrosion products such as $Zn_5(OH)_8Cl_2 \cdot H_2O$ and Al_2O_3.

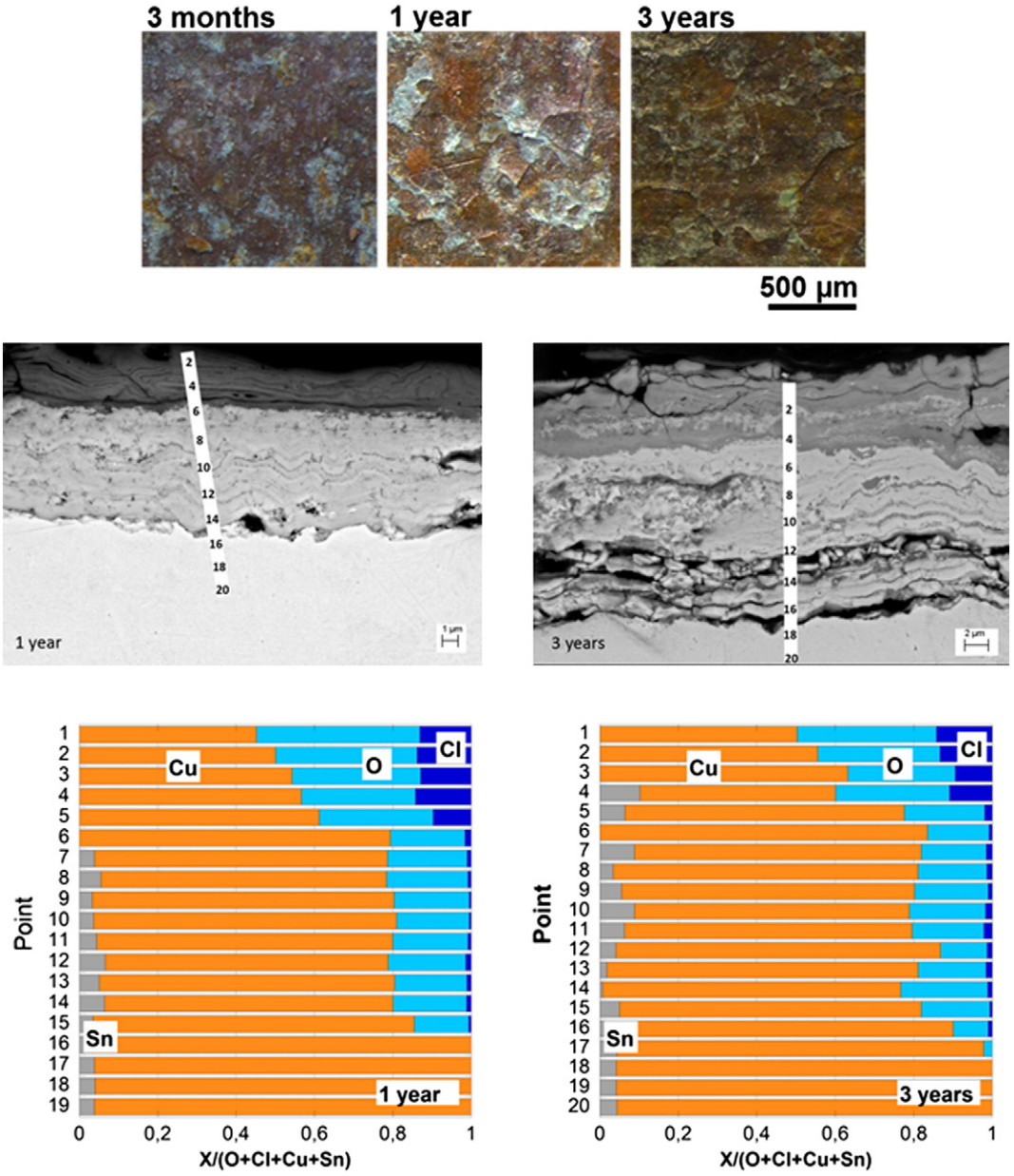

Fig. 8. Visual appearance of the Cu4Sn alloy illustrated after 3 months, 1 and 3 years of exposure at site 1 (high deposition rates of chlorides) (top) and cross-sections of the corrosion patina after 1 and 3 years (middle) and corresponding relative elemental mass distributions based on EDS analysis (bottom).

As mentioned in the previous section on visual appearance, the color of Cu sheet, Cu4Sn and Cu15Zn reached a more brown-greenish appearance after 3 years of exposure, while the Cu5Al5Zn alloy retained a more lustrous goldish color without any signs of the characteristic blue-greenish color of regular copper patina. The surface appearance of any corrosion products is influenced by several physiochemical properties, such as the ability of the light to be reflected by the surface or to pass through the corrosion product. Other important factors are the body color of the corrosion product, trace amounts of impurities that may change the optical properties and interference effects when the electromagnetic radiation interacts with the corrosion products. It is beyond the scope of this paper to discuss the surface appearance of current corroded copper alloy surfaces but it is evident that one main cause of the much more lustrous surface appearance of Cu5Al5Zn compared to that of the other materials is the thinner layer of patina on the Cu5Al5Zn alloy (1–2 µm) compared with that on Cu sheet, Cu15Zn and Cu4Sn (8–20 µm). A more detailed spectrophotometric evaluation of changes in surface coloration will follow in a next-coming paper by the authors.

Observed differences between copper sheet and the copper-alloys exposed at the different test sites were evident not only from differences in visual appearance and measured corrosion rates, but also from the extent of flaking of loosely adherent corrosion products, illustrated after 1 and 3 years for Cu sheet and Cu4Sn at site 1, Fig. 12. Flaking (predominantly of blue-greenish products) was particularly severe for Cu4Sn and Cu sheet, but only minor or non-significant for Cu15Zn and Cu5Al5Zn, respectively. The presence of loosely adherent corrosion products, easily flaked from the surface on Cu sheet and Cu4Sn, was predominantly observed at sites 1 and 2, i.e. at the sites with the highest deposition rates of chlorides. Only minor effects of flaking were evident for the same materials exposed at sites 3 and 4. In-depth mechanistic studies of these spalling processes will be discussed in a subsequent paper by the authors.

In summary, Cu sheet and Cu4Sn formed loosely adherent non-heterogeneous greenish-blue corrosion products that easily flaked from

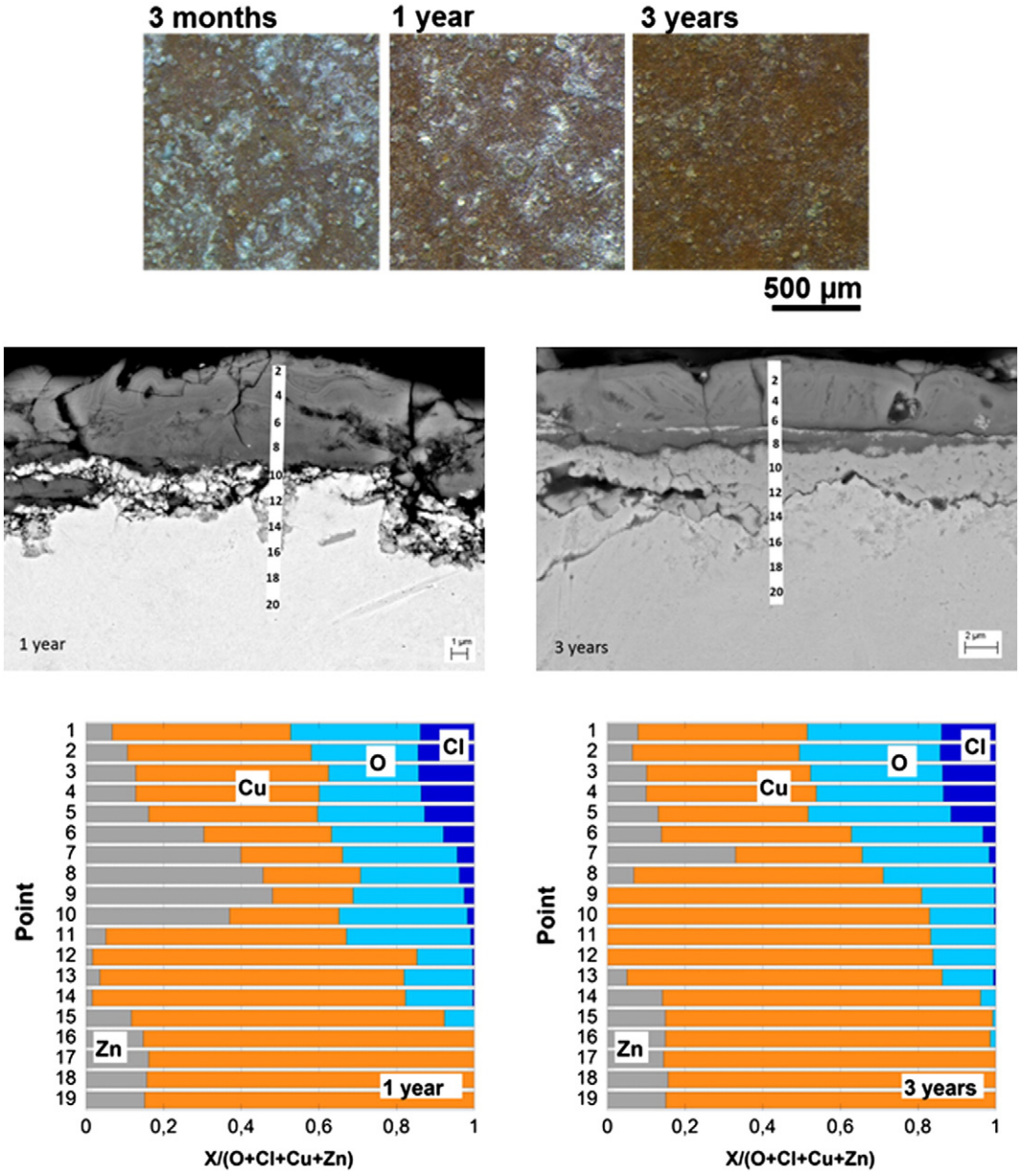

Fig. 9. Visual appearance illustrated after 3 months, 1 and 3 years of exposure at site 1 (high deposition rates of chlorides) (top) and cross-sections of corrosion patina formed on the Cu15Zn alloy after 1 and 3 years (middle) and corresponding relative elemental mass distributions based on EDS analysis (bottom).

the surface whereas the Cu15Zn and Cu5Al5Zn alloys formed a more adherent patina layer with significantly less tendency of spallation. Flaking was mainly attributed to the presence of nantokite within the patina of Cu sheet and Cu4Sn that gradually transformed into the more voluminous corrosion product of paratacamite, inducing internal physical stresses within the patina (Krätschmer et al., 2002; Scott, 2002). This process was facilitated by the porous nature of the patina allowing penetration of moisture and oxygen (Scott, 2002). Observed findings imply that the Cu15Zn and Cu5Al5Zn alloys are less sensitive to chloride-induced atmospheric corrosion compared with Cu sheet and Cu4Sn. The confirmed presence of Zn/Zn–Al chloride rich corrosion products within the patina is suggested to improve its barrier properties as well as the possibility for zinc to stabilize paratacamite. The conditions for forming nantokite is more hindered on CuZn15 and Cu5Al5Zn than on Cu sheet and Cu4Sn, resulting in reduced chance of flaking on Cu15Zn and Cu5Al5Zn.

3.5. Release rates of copper and the main alloy constituents at site 2

Continuous monitoring of metal release of copper and the main alloying elements (Cu4Sn:tin, Cu15Zn: zinc, Cu5Al5Zn: tin, zinc, aluminum, iron) was performed during five years from copper sheet and the three copper-based alloys at site 2. Even though the release investigation did not start at the same time as the reported corrosion rate and corrosion product evolution study, prevailing environmental conditions, rainfall quantities and corresponding corrosivity classes were for these time periods very similar. Annual release rates of copper and the main alloying constituents per given surface area are compiled for each year of the five-year exposure in Fig. 13 (top). Total metal release rates after one year of exposure were significantly lower compared with measured corrosion rates for all materials, 92, 96, 92% lower for Cu sheet, Cu4Sn, and Cu15Zn, respectively and 69% lower for Cu5Al5Zn. The results further show time dependent release

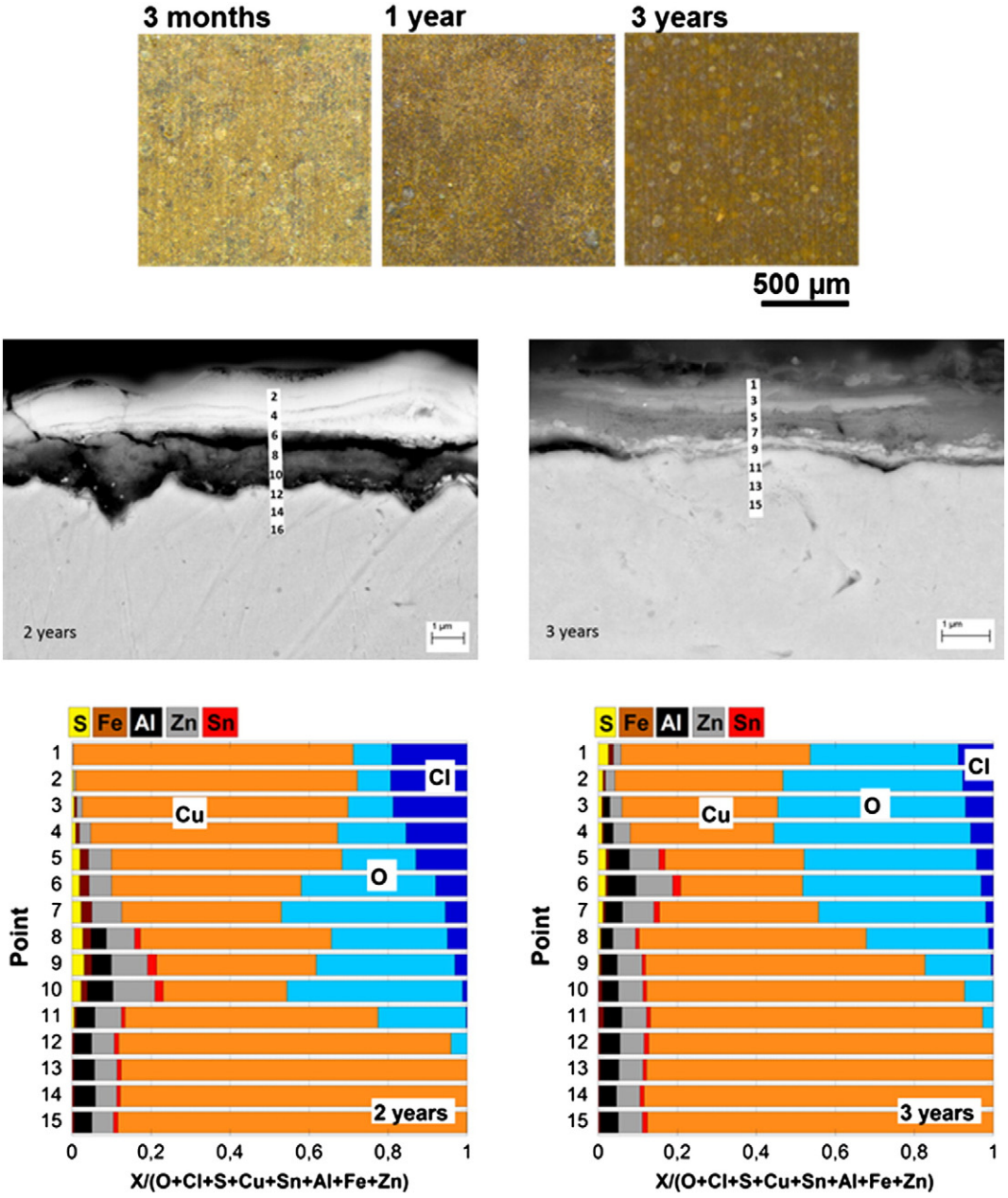

Fig. 10. Visual appearance illustrated after 3 months, 1 and 3 years of exposure at site 1 (high deposition rates of chlorides) (top) and cross-sections of corrosion patina formed on the Cu5Al5Zn alloy after 2 and 3 years and corresponding relative elemental mass distribution based on EDS analysis.

rates without the same ranking between the materials as observed for the corrosion rates (Cu4Sn — the highest, Cu5Al5Zn — the lowest). The runoff rate of copper after one year followed the order: Cu sheet (1.4 g m^{-2} y^{-1}) > Cu4Sn (1.0 g m^{-2} y^{-1}) > Cu5Al5Zn (0.77 g m^{-2} y^{-1}) > Cu15Zn (0.46 g m^{-2} y^{-1}). Annual rates during the fifth year showed a shifted order: Cu15Zn (0.52 g m^{-2} y^{-1}) > Cu5Al5Zn (0.42 g m^{-2} y^{-1}) > Cu4Sn (0.28 g m^{-2} y^{-1}) (Cu sheet excluded due to different exposure period). Observed differences are attributed to changes in the outermost patina composition and characteristics with time.

To allow comparisons between different years of varying annual rainfall quantities, the annual release rate was normalized to this quantity, Fig. 13 (bottom). The results clearly reveal reduced release rates of copper with time for Cu sheet, an effect also observed for the Cu4Sn alloy after three years of very similar released quantities per given rainfall unit. This is believed to be attributed to the gradual formation of a patina with very similar outermost surface composition (predominantly paratacamite/atacamite) with time. The presence of tin oxides within the patina of Cu4Sn is of less importance for the release process as this is predominantly governed by a combination of chemical dissolution/re-precipitation processes at the surface patina and the action by impinging rainfall and its characteristics. These processes are described elsewhere (He et al., 2001). As previously shown for the Cu15Zn alloy, zincite and hydrozincite as well as cuprite and paratacamite/atacamite were present in the surface patina up to 1 year of exposure. The surface coverage of copper rich corrosion products compared with zinc-rich products gradually increased with time due to selective release of zinc and as a consequence an increased release of copper, Fig. 13 (bottom). Similar dezincification processes for different brass alloys have been described elsewhere (Goidanich et al., 2011). Reduced release of zinc was evident during the fourth year of exposure and only a minor amount of zinc was released during the fifth year. During the last year was the annual release rate of copper

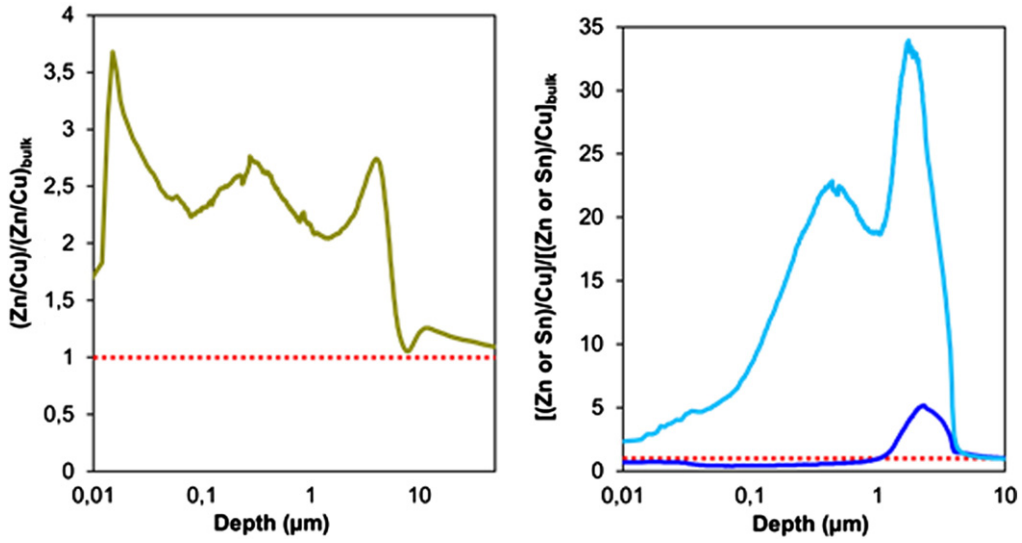

Fig. 11. Enrichment of zinc in the patina compared with its bulk content in relation to copper for the Cu15Zn alloy determined by means of GDOES (left) and corresponding enrichment of zinc (light blue - upper curve) and tin (dark blue - lower curve) for the Cu5Al5Zn alloy (right).

relatively similar to rates e.g. the Cu4Sn alloy exposed in parallel. This shows that the patina composition at the utmost surface with time became more and more similar to the patina formed on Cu sheet and Cu4Sn.

Despite significantly lower corrosion rates compared with the other materials, cf. Fig. 5, comparable release rates of copper were determined from the Cu5Al5Zn alloy as determined for Cu sheet and the other alloys. This clearly illustrates that even though zinc, tin and aluminum-rich corrosion products were enriched at the bulk/patina interface, reducing their corrosion rates, their presence in the outermost surface patina was minor and hence their influence on the release process limited. The release of the alloy constituents (tin, zinc, aluminum, iron) was gradually reduced with time and corresponded to 7% of the total released amount of metals after 5 years.

In all, both the Cu15Zn and the Cu5Al5Zn alloys revealed preferential release of zinc, i.e. significant dezincification (higher released amount of zinc to copper ratio compared with corresponding bulk ratio) during the first year that was gradually reduced with time and the gradual formation of a more compact patina with predominantly copper-rich corrosion products in the outermost surface layer with reduced solubility properties with time.

Despite significantly slower corrosion rates for the Cu5Al5Zn alloy compared with Cu sheet, Cu4Sn and Cu5Al5Zn, observed runoff rates of copper were similar after five years of exposure.

4. Conclusions

Four outdoor test sites located in the Brest region, France, have been used to investigate the influence of chloride deposition on corrosion effects and metal release rates of bare copper sheet (Cu sheet) and the three commercial Cu-based alloys Cu15Zn, Cu4Sn and Cu5Al5Zn.

The test sites are characterized by chloride deposition rates that vary by a factor 40 to 70 between the highest (<5 m from the coastal line) and the lowest chloride load (40 km from the coast). The corresponding corrosion mass losses of copper during the first year of unsheltered exposure at 45°, south, range from 24.4 to 8.9 g/m^2. The data for all four sites agree reasonably well with the corresponding estimated copper corrosion rates according to the ISO standard 9223.

The corrosion rates during the first year at the site with highest chloride load varied almost by a factor of ten between the investigated materials: Cu4Sn (38.3 g m^{-2} y^{-1}) > Cu sheet (24.4 g m^{-2} y^{-1}) > Cu15Zn (19.4 g m^{-2} y^{-1}) > Cu5Al5Zn (4.1 g m^{-2} y^{-1}). The corrosion rates of all four materials decrease continuously with distance from the coast, i.e. with decreasing chloride load.

The patina of copper and the copper-based alloys was composed of two main layers, Cu_2O as the inner layer and $Cu_2(OH)_3Cl$ as the outer layer, possibly sandwiched with the discontinuous presence of CuCl. Additional minor patina constituents were SnO_2 (Cu4Sn),

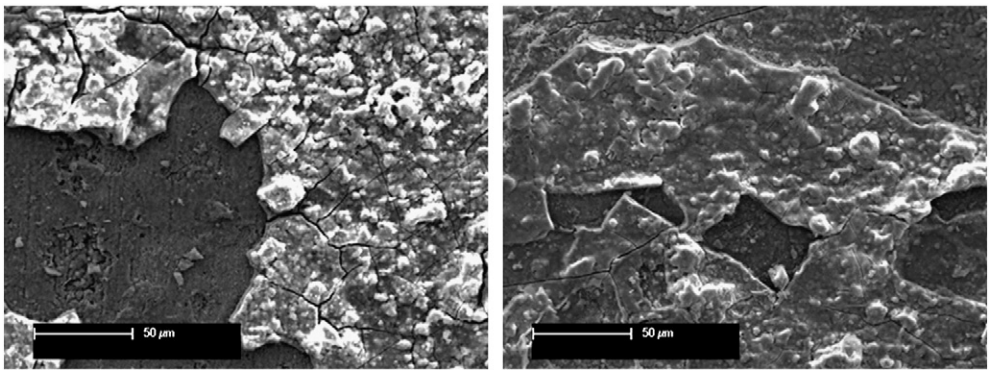

Fig. 12. SEM image of Cu sheet (left) and Cu4Sn (right) surfaces with loosely adherent green-bluish corrosion products (white flakes) after 1 and 3 years, respectively, of unsheltered exposure at site 1 (high deposition rates of chlorides).

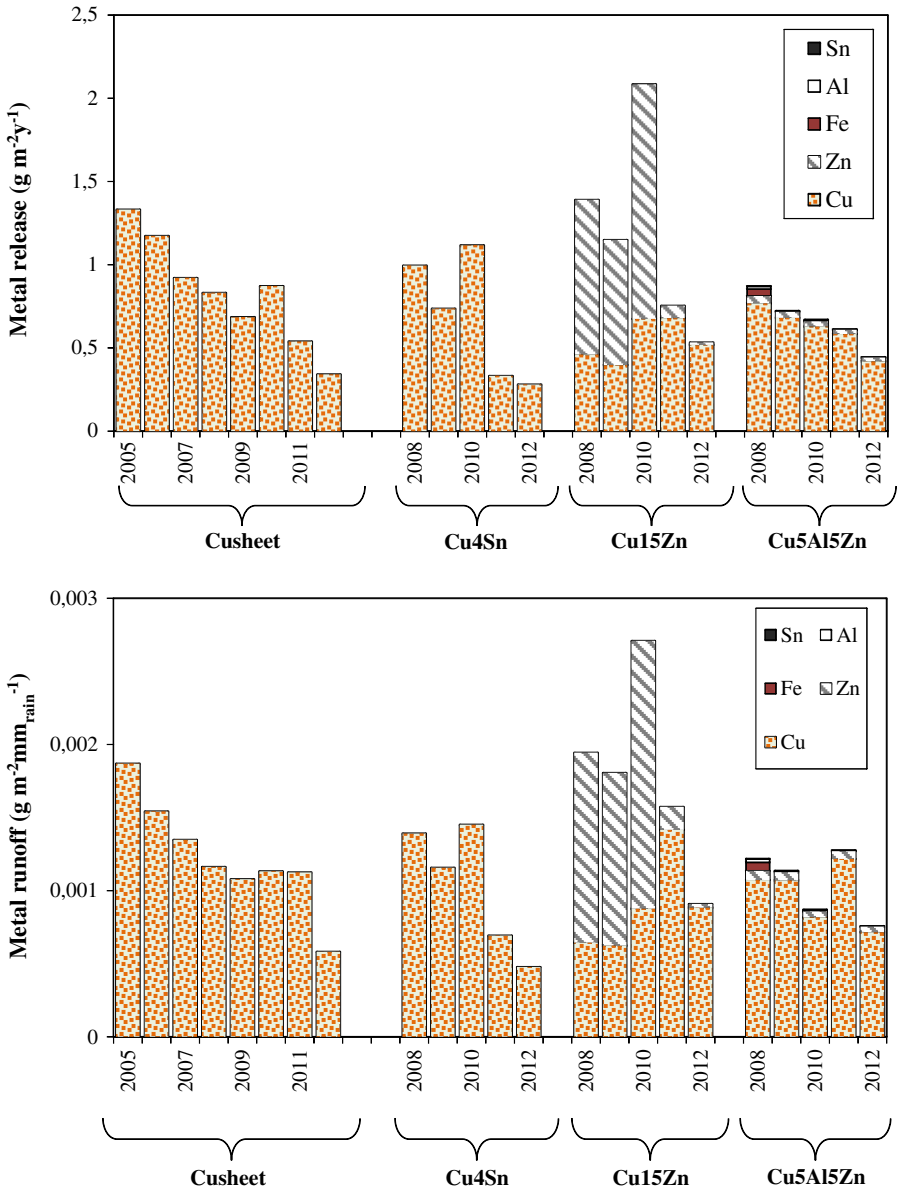

Fig. 13. Annual release rates of copper (Cu) and bulk alloy constituents (Zn, Al, Fe, Sn) for Cu sheet (8 years) and the alloys Cu4Sn, Cu15Zn and Cu5Al5Zn (5 years) normalized to surface area (top) and surface area and annual rainfall quantity impinging the surfaces (bottom). All materials were exposed at site 2 (St Anne).

$Zn_5(OH)_6(CO_3)_2$ (Cu15Zn) and $Zn_6Al_2(OH)_{16}CO_3 \cdot 4H_2O/Zn_2Al(OH)_6Cl \cdot 2H_2O/Zn_5Cl_2(OH)_8 \cdot H_2O$ and Al_2O_3 (Cu5Al5Zn). The observed Zn- and Zn/Al-containing corrosion products may act as barrier layers to protect the Cu15Zn and Cu5Al5Zn alloys against chloride-induced corrosion. They are important factors to explain why Cu15Zn and Cu5Al5Zn are less sensitive to chloride-induced atmospheric corrosion than Cu sheet and Cu4Sn.

The outer patina layer became more compact and adhering to the underlying oxide with time, causing a continuous decrease in corrosion rate with exposure time for all four exposure sites and materials. Flaking of the outer, weakly adhering, patina layer was observed on Cu4Sn and Cu sheet, to a much lesser extent on the Cu15Zn alloy, and not at all on the Cu5Al5Zn alloy. Flaking was mainly attributed to the formation of CuCl, which can transform to $Cu_2(OH)_3Cl$ upon reaction to moisture and oxygen and cause physical stress within the patina layer.

The total patina layer thickness on all four materials followed the same order as the corrosion rates, ranging from about 20 μm (Cu4Sn) to less than 2 μm (Cu5Al5Zn). The patina thickness was a major factor to influence the visual appearance, i.e. causing the Cu5Al5Zn alloy a lustrous goldish appearance still after three years of exposure, while the other copper-based materials appeared more brownish–greenish.

Observed total release rates were significantly lower than the corrosion rates for all materials, 92, 96, and 92% lower for Cu sheet, Cu4Sn, and Cu15Zn, respectively and 69% lower for Cu5Al5Zn after the first year of exposure, and did not show the same ranking between the materials as observed for the corrosion rates (Cu4Sn — the highest, Cu5Al5Zn — the lowest). The release rate of copper after one year followed the order: Cu sheet (1.4 g m^{-2} y^{-1}) > Cu4Sn (1.0 g m^{-2} y^{-1}) > Cu5Al5Zn (0.77 g m^{-2} y^{-1}) > Cu15Zn (0.46 g m^{-2} y^{-1}). This order changed with time and revealed relatively similar rates during the fifth year of exposure: Cu15Zn (0.52 g m^{-2} y^{-1}) > Cu5Al5Zn (0.42 g m^{-2} y^{-1}) > Cu4Sn (0.28 g m^{-2} y^{-1}) (Cu sheet excluded due different starting period).

The overall composition of the outer part of the patina layer and its solubility properties were major factors that influence the extent of released metals from the investigated materials.

Acknowledgment

Financial support from the European Copper Institute (ECI) for long-term fundamental studies of atmospheric corrosion of copper and copper-based alloys is highly acknowledged.

The authors are also very grateful to Jon Brunk, Div. Surface and Corrosion Science, KTH for his invaluable efforts during field exposure initiation and to Jean Michel Hamoignon, Cécile Hall-Fournier, Vanessa Le Verne and Melen Le Moigne, Institut de la Corrosion, Brest, France, for their tireless and dedicated work maintaining the test sites and collecting samples. Alexander Mörsdorf, KTH is acknowledged for the literature survey. Oskar Karlsson and Mats Randelius at Swerea Kimab, Stockholm, Sweden, are acknowledged for generating SEM/EDS linescans and GDOES depth profiles, respectively.

References

Bertolotti G, Bersani D, Lottici PP, Alesiani M, Malcherek T, Schlueter J. Micro-Raman study of copper hydroxychlorides and other corrosion products of bronze samples mimicking archaeological coins. Anal Bioanal Chem 2012;402:1451–7.

Cao X, Xu C. Synergistic effect of chloride and sulfite ions on the atmospheric corrosion of bronze. Mater Corros 2006;57:400–6.

Cao X, Wang N, Liu N. Synergistic effect of chloride and NO_2 on the atmospheric corrosion of bronze. Anti-Corros Method M 2009;56:299–305.

Chen ZY, Persson D, Nazarov A, Zakipour S, Thierry D, Leygraf C. In situ studies of the effect of CO_2 on the initial NaCl-induced atmospheric corrosion of copper. J Electrochem Soc 2005a;152:B342–51.

Chen ZY, Persson D, Samie F, Zakipour S, Leygraf C. Effect of carbon dioxide on sodium chloride-induced atmospheric corrosion of copper. J Electrochem Soc 2005b;152:B502–11.

Chen ZY, Zakipour S, Persson D, Leygraf C. Combined effects of gaseous pollutants and sodium chloride particles on the atmospheric corrosion of copper. Corrosion 2005c;61:1022–34.

Chen ZY, Persson D, Leygraf C. Initial NaCl-particle induced atmospheric corrosion of zinc—effect of CO2 and SO2. Corros Sci 2008;50:111–23.

Cole IS, Ganther W, Paterson DA, King G, Furman SA, Lau D. Holistic model for atmospheric corrosion: part 2 — experimental measurement of deposition of marine salts in a number of long range studies. Corros Eng Sci Technol 2003;38:259–66.

Cole IS, Lau D, Paterson DA. Holistic model for atmospheric corrosion part 6 — from wet aerosol to salt deposit. Corros Eng Sci Technol 2004;39:209–18.

Cole I, Azmat N, Kanta A, Venkatraman M. What really controls the atmospheric corrosion of zinc? Effect of marine aerosols on atmospheric corrosion of zinc. Int Mater Rev 2009;54:117–33.

Constantinides I, Adriaens A, Adams F. Surface characterization of artificial corrosion layers on copper alloy reference materials. Appl Surf Sci 2002;189:90–101.

Costas LP. Atmospheric corrosion of copper alloys exposed for 15 to 20 years. In: Dean Jr SW, Rhea EC, editors. Atmopsheric Corrosion of Metals, ASTM STP 767America Society for Testing and Materials; 1982. p. 106–15.

Cramer SD, Matthes SA, Covino BS, Bullard SJ, Holcomb GR. Environmental factors affecting the atmospheric corrosion of copper. In: Townsend HE, editor. Outdoor atmospheric corrosion, 1421. W Conshohocken: American Society Testing and Materials; 2002. p. 245–64.

Davis JR. Engineering properties and service characteristics. In: Davis JR, editor. Copper and copper alloysASM International; 2001. p. 385–418.

De la Fuente D, Simancas J, Morcillo M. Morphological study of 16-year patinas formed on copper in a wide range of atmospheric exposures. Corros Sci 2008;50:268–85.

Feliu S, Morcillo M, Chico B. Effect of distance from sea on atmospheric corrosion rate. Corrosion 1999;55:883–91.

Frost RL. Raman spectroscopy of selected copper minerals of significance in corrosion. Spectrochim Acta A Mol Biomol Spectrosc 2003;59:1195–204.

Ghoniem M. The characterization of a corroded Egyptian bronze statue and a study of the degradation phenomena. Int J Conserv Sci 2011;2:95–108.

Goidanich S, Odnevall Wallinder I, Arenas MA, De Damboreneac J, Ormellese M, Sánchez Amaya SM, et al. Effect of the envioronment on the metal release and corrosion behavious of different copper-based alloys: field exposures at 5 different test sites in Europe. 17th International Corrosion Congress, Las Vegas, US Paper 2192; 2008.

Goidanich S, Brunk J, Herting G, Arenas MA, Odnevall Wallinder I. Atmospheric corrosion of brass in outdoor applications: patina evolution, metal release and aesthetic appearance at urban exposure conditions. Sci Total Environ 2011;412–413:46–57.

Hayez V, Costa V, Guillaume J, Terryn H, Hubin A. Micro Raman spectroscopy used for the study of corrosion products on copper alloys: study of the chemical composition of artificial patinas used for restoration purposes. Analyst 2005;130:550–6.

He W, Odnevall Wallinder I, Leygraf C. A comparison between corrosion rates and runoff rates from new and aged copper and zinc as roofing material. Water Air Soil Pollut 2001;1:67–82.

Holm R, Mattsson E. Atmospheric corrosion tests of copper and copper alloys in Sweden — 16-year results. In: Dean Jr SW, Rhea EC, editors. Atmopsheric corrosion of metals, ASTM STP 767America Society for Testing and Materials; 1982. p. 85–104.

ISO. ISO 9225 Corrosion of metals and alloys – corrosivity of atmospheres – measurement of environmental parameters affecting corrosivity of atmospheres; 2012a.

ISO. ISO 17752: corrosion of metals and alloys — procedures to determine and estimate runoff rates of metals from materials as a result of atmospheric corrosion; 2012b.

ISO. ISO 9226: corrosion of metals and alloys – corrosivity of atmospheres – determination of corrosion rate of standard specimens for the evaluation of corrosivity; 2012c.

ISO. ISO 9223: corrosion of metals and alloys – corrosivity of atmospheres – classification, determination and estimation; 2012d.

Kosec T, Ropret P, Legat A. Raman investigation of artificial patinas on recent bronze — part II: urban rain exposure. J Raman Spectrosc 2012;43:1587–95.

Krätschmer A, Odnevall Wallinder I, Leygraf C. The evolution of outdoor copper patina. Corros Sci 2002;44:425–50.

LeBozec N, Thierry D, Rohwerder M, Persson D, Luckeneder G, Luxem L. Effect of carbon dioxide on the atmospheric corrosion of Zn–Mg–Al coated steel. Corros Sci 2013;74:379–86.

Leygraf C, Graedel T. Atmospheric corrosion. New York: John Wiley & Sons; 2000.

Mattsson E. Corrosion of copper and brass — practical experiencce in relation ro basic data. Br Corros J 1980;15:6–13.

Morcillo M, Almeida E, Marrocos M, Rosales B. Atmospheric corrosion of copper in Ibero-America. Corrosion 2001;57:967–80.

Neufeld AK, Cole IS, Bond AM, Furman SA. The initiation mechanism of corrosion of zinc by sodium chloride particle deposition. Corros Sci 2002;44:555–72.

Ospitali F, Chiavari C, Martini C, Bernardi E, Passarini F, Robbiola L. The characterization of Sn-based corrosion products in ancient bronzes: a Raman approach. J Raman Spectrosc 2012;43:1596–603.

Scholes IR, Jacob WR. Atmospheric corrosion of copper and copper-base alloys during twenty years' exposure in a marine and industrial environment. J Inst Met 1970;98:272–80.

Scott DA. A review of copper chlorides and related salts in bronze corrosion and as painting pigments. Stud Conserv 2000;45:39–53.

Scott DA. Chlorides and basic chlorides. In: Scott DA, editor. Copper and bronze in art — corrosion, colorants, conservation. Los Angeles: Getty Publications; 2002.

Sequeira CAC. Copper and copper alloys. In: Revie RW, editor. Uhlig's corrosion handbook. John Wiley & Sons; 2011.

Strandberg H, Johansson LG. Some aspects of the atmospheric corrosion of copper in the presence of sodium chloride. J Electrochem Soc 1998;145:1093–100.

Tidblad J. Atmospheric corrosion of metals in 2010–2039 and 2070–2099. Atmos Environ 2012;55:1–6.

Volovitch P, Vu TN, Allély C, Abdel Aal A, Ogle K. Understanding corrosion via corrosion product characterization: II. Role of alloying elements in improving the corrosion resistance of Zn–Al–Mg coatings on steel. Corros Sci 2011;53:2437–45.

Watanabe M, Toyoda E, Handa T, Ichino T, Kuwaki N, Higashi Y, et al. Evolution of patinas on copper exposed in a suburban area. Corros Sci 2007;49:766–80.

Zhang X, Leygraf C, Odnevall Wallinder I. Atmospheric corrosion of Galfan coatings on steel in chloride-rich environments. Corros Sci 2013;73:62–71.